



Effect of friction stir welding on mechanical and microstructural properties of AISI 316L stainless steel butt joints

S. Shashi Kumar¹ · N. Murugan² · K. K. Ramachandran³

Received: 2 December 2017 / Accepted: 21 June 2018 / Published online: 29 June 2018
© International Institute of Welding 2018

Abstract

Friction stir welding (FSW) was applied for the joining of 3-mm-thick AISI 316L stainless steel sheets. The investigation was aimed to explore the relationship between weld joint characteristics and one of the very important primary FSW parameters, the welding speed. The soundness of the fabricated joints was tested by x-ray radiography technique initially. The microstructural studies of the joints were carried out using scanning electron microscopy (SEM), transmission electron microscopy (TEM) and electron back scattered diffraction (EBSD). Discontinuous dynamic recrystallization was the suggestive dominant recrystallization mechanism in the weld stir zone (SZ). The presence of fine equiaxed austenite grain boundaries and the consequent increase in hardness at the weld SZ resulted in joint strength superior to that of the base steel at higher welding speeds. But, at lower welding speeds, the evolution of delta ferrite decreased the toughness and strength of the joints owing to higher heat generation (higher peak temperature). However, the delta ferrite formed in the weld SZ has not transformed into sigma phase, probably due to fast cooling of the weld zone.

Keywords Friction stir welding · Mechanical properties · Welding speed · Microstructural properties · Austenitic stainless steel · Delta ferrite

1 Introduction

Austenitic stainless steels generally exhibit a combination of unique properties such as high strength at elevated temperatures, better corrosion resistance, high ductility and good toughness at low temperatures. These distinctive properties

make austenitic stainless steels the most desirable material in industrial sectors such as ship building, food processing, petrochemical, and nuclear power generation for the fabrication of the various parts and structures [1, 2]. As a result, the total ingestion of austenitic stainless steel was estimated to be about 70% of the total stainless steel consumption (<https://masteel.co.uk/news/popular-grades-stainless-steel-304-316-2/>).

With regard to the fusion welding of austenitic stainless steels, Yan et al. [3] studied the performance of AISI 304 stainless steel weld joints using gas tungsten arc welding (GTAW), laser and GTAW-laser hybrid welding processes. The results of experimental analysis revealed that the characteristics of the laser-welded joints were superior over the GTAW and GTAW-laser hybrid-welded joints. But, at the weld zone, they found a greater concentration of delta ferrite in the laser-welded joints, which was attributed to higher heat input. Feng et al. [4] demonstrated a methodology for carrying out keyhole gas tungsten arc welding of thick AISI 316L plates and found that the weld zone was comprised of a mixture of austenite and delta ferrite. The authors speculated that the formation of delta ferrite in the weld zone was the consequence of higher heat generation (peak temperature) that deteriorated the mechanical properties of the weld joints. The

Recommended for publication by Commission III - Resistance Welding, Solid State Welding, and Allied Joining Process

✉ S. Shashi Kumar
shashiraj07@gmail.com

N. Murugan
dmurugan@hotmail.com

K. K. Ramachandran
kkramachandran@gectcr.ac.in

¹ School of Mechanical Engineering, SRM Institute of Science and Technology, Kattankulathur, Tamil Nadu 603203, India

² Department of Robotics and Automation Engineering, PSG college of Technology, Coimbatore, Tamil Nadu 641004, India

³ Department of Mechanical Engineering, Government Engineering College, Thrissur, Kerala 680009, India

weldability studies of 316L stainless steel joints using resistance spot welding was reported by Kocabekir et al. [5]. The authors found that the joint strength was influenced by the weld cycle time. The higher weld cycle time not only produced higher joint strength but also gradually increased the weld nugget diameter leading to coarsening of grains at the nugget zone and heat-affected zone (HAZ). Gowrishankar et al. [6] performed joining of AISI 316L stainless steel plates using submerged arc welded process with 5, 9 and 13 passes. The results showed that with increase in the number of passes, the hardness and tensile properties of the welds were improved, whereas the ductility and toughness of the joints got deteriorated. The variations in the mechanical properties were attributed to the abrupt microstructural changes, particularly the amount, morphology and distribution of the delta ferrite in the weld nugget.

Owing to the high coefficient of thermal expansion and lower thermal conductivity of austenitic stainless steel, the fusion weld austenitic stainless steel joints are more prone to hot cracking [7, 8]. Hot cracking pave way to cause crevice corrosion and in turn affects the fatigue life of the fusion-welded joints. Also, higher heat input leads to the formation of delta ferrite at the weld zone, which was the precursor for the formation of chromium carbides and sigma phases that degraded the toughness and strength of the fusion-welded joints [9]. From the literature, it is very clear that higher heat input (higher welding temperature at the weld nugget and HAZ) are more detrimental to cause adverse changes in the physical, mechanical and metallurgical characteristics of the welds and in turn resulted in the premature failure of the joints [10–12]. The consequence of higher heat input can be controlled up to a certain extent by taking primitive measures such as fine tuning of the welding input parameters, but the release of harmful gases such as hexavalent chromium enriched fumes owing to boiling of weld pool can lead to serious risk of respiratory and cancer disorders in welders [13, 14]. This has forced researchers to explore the possibility of solid state welding processes for welding of austenitic stainless steels.

Friction stir welding (FSW) is one such solid-state welding process, invented at The Welding Institute (TWI), UK, by Thomas et al. [15] for the joining of aluminium alloys. It uses a non-consumable rotating tool which is plunged at the joint line of the abutting surfaces and traverse along the joint line to produce solid-state bonding between the plates. FSW of aluminium alloys is now well-established and commercially implemented in many manufacturing sectors. Also, over a decade, FSW was successfully demonstrated in joining of high melting temperature (HMT) materials like steels and stainless steels. The development of FSW tool materials made of super abrasives or a combination of high refractory materials that exhibit superior qualities such as elevated temperature hardness, higher toughness and better wear resistance has proved its competency in successful joining of HMT materials.

With regard to FSW of austenitic stainless steels, a few works are reported in the literature. Meshram et al. [16] performed FSW of 4-mm-thick 316L stainless steel to study the mechanical properties of the welded joints. Experimental trials were carried out at a few combinations of tool rotational and welding speeds and the joints produced at tool rotational speed of 1100 rpm and welding speed of 8 mm/min had exhibited the highest joint efficiency of 104%. Meran et al. [17] studied the FS welding feasibility of 2.5-mm-thick 304 stainless steel using a tungsten-based tool material. FSW trials were carried out at tool rotational speed of 1000 rpm by varying the welding speed between 40 and 100 mm/min. They reported higher joint strength of 485 MPa for joints produced at tool rotational speed of 1000 rpm and welding speed of 63 mm/min. Kokowa et al. [18] studied the microstructural evolution of friction stir-welded 304 stainless steel plates with two different thickness (2 and 6 mm). The plates were FS welded at two different welding speed/tool rotational speed combinations; viz. $4.5 \text{ mms}^{-1}/1300 \text{ rpm}$ and $1.3 \text{ mms}^{-1}/550 \text{ rpm}$. They reported that the SZ and thermomechanically affected zone (TMAZ) consisted of equiaxed and recovered microstructure. Also, delta ferrite and sigma phase was evidenced during transmission electron microscopy analysis at the weld SZ and they construed that the secondary phase formation is highly influenced by the rate of cooling of the weld zone. Meran and Caryurt [19] performed FS welding of 304 stainless steel by varying the tool rotational speed, welding speed, axial forces and tool tilt angles. The authors reported that the peak tensile strength of 430 MPa (85% of the base steel) was obtained under the welding condition; tool rotational speed of 950 rpm, welding speed of 60 mm/min, axial force of 9 kN and tool tilt of 1.5° . The authors reported that the weld SZ consisted of equiaxed grains and the transition zone consisted of dark shear bands with Cr_2O_3 layers.

Friction stir processing (FSP) of AISI 316L stainless steel of 15-mm-thick plate was carried out by Chen et al. [20] and primarily studied the significance of banded structures in the processed zone. The FSP was carried out for the three different sets of processing parameters with rotational speeds of 4, 5 and 6 rad/s; traverse speeds of 16, 20 and 24 mm/min and tool working loads of 25, 30 and 35 kN. They found that the banded structure in the processed zone consisted of sigma precipitates and the formation was influenced by the heat generation. Their studies concluded that the proper choice of FSP parameters (such as lower tool rotational speed, higher welding speeds and lower working loads) could restrain the possibilities of sigma phase precipitation in the weld zone. Hajian et al. [21] studied the microstructural and mechanical properties of friction stir processed AISI 316L stainless steel of 2-mm-thick for a constant transverse speed of 63 mm/min and varying tool rotational speeds of 200 and 315 rpm. Their studies revealed that lower tool rotational speed was more beneficial for the evolution of equiaxed grains in the stir zone (SZ), which

Table 1 Chemical composition of AISI 316L stainless steel

Element	C	Mn	S	P	Si	Ni	Cr	N	Mo	Fe
wt%	0.02	0.8	0.004	0.04	0.28	12.07	16.58	0.035	2.02	Bal

consequently increased the hardness and strength of the processed zone than the base steel.

It can be summarised that the reported literatures on FSW/FSP of austenitic stainless steel are mostly typical cases that explored the mechanical and microstructural properties against a single or a few discrete combinations of FSW/FSP process parameters. Comprehensive studies on FSW of AISI 316L stainless steel that correlates the mechanical properties and microstructural evolution of the joints with the primary FSW process parameters is missing in the literatures. Therefore, in the present study, FSW was applied for joining of AISI 316L stainless steel sheets in the butt configuration and the microstructural evolution and mechanical properties of the joints were correlated with the welding speed (tool traverse speed).

2 Experimental procedure

3-mm thick, AISI 316L austenitic stainless steel rolled sheet was used as the base material for the present study. The tested chemical composition and mechanical properties of the as-received base steel sheet are given in Tables 1 and 2, respectively.

The scanning electron and optical micrographs of the base steel (in the as-received condition) are shown in Fig. 1. The base steel consists of mostly coarse austenite grains with tiny amounts of ferrite. Annealed twins were observed crossing the grain boundaries. By the mean linear intercept (MLI) method, average grain size of the base steel was found to be $28 \pm 5 \mu\text{m}$. The base sheet was sheared to rectangular size of $100 \text{ mm} \times 50 \text{ mm}$, such that the 100 mm side lies in the rolling direction. A semi-automatic FSW machine (manufactured by M/s. R.V. Machine tools, Coimbatore, India) modified by installing a refrigerating unit for cooling the spindle head assembly (to alleviate excessive heating of the tool holder and spindle bearings) was used for the welding trials. The FSW tool was developed using a tungsten lanthanum (99% W–1% La_2O_3) alloy [22]. The tool geometry consists of a plain shoulder of 18-mm diameter with conical pin of 8 and 6 mm root and tip diameters, respectively, and pin height of 2.8 mm as shown in Fig. 2.

The samples were welded by varying the welding speed from 25 to 100 mm/min with increments of 25 mm/min while keeping the other primary FSW parameters at constant values. The constant values of other parameters fixed by initial trials were tool rotational speed of 600 rpm, axial force of 12 kN and tool tilt angle of 1.5° . In order to prevent oxidation of the base material, argon inert gas at 15 lpm was supplied into the weld zone. A K-type thermocouple sensor installed in the oil hardened steel backing plate using silver paste was used to record the temperature at the middle of the weld. A hole of 1.5-mm diameter was drilled approximately at the centre of the backing plate such that the thermocouple bead stay in flush with the backup plate surface just under the joint line. The FS-welded joints produced were inspected using x-ray radiography non-destructive test to assess whether the joints are defect-free, internally.

For microstructural analysis, optical microscopy, using Mitutoyo; model: BX 51 optical microscope and scanning electron microscopy using Carl Zeiss, Germany; model: SIGMA HV field emission scanning electron microscope (FESEM) interfaced with BRUKER QUANTAX 200 – Z10 EDS detector were used. Orientation imaging microscopy (OIM) model: FEI quanta FEG 200 equipped with FESEM, was used to determine grain features like average grain size and grain misorientation in a scan area of $132 \times 99 \mu\text{m}$ at a step size of $2.5 \mu\text{m}$. For TEM analysis, Philips CM 12 microscope was used and operated at 120 kV. The thin disc-shaped TEM test specimens were prepared via twin jet electrolytic thinning technique by immersing in a solution with 10% HClO_4 + 90% ethanol at 50 V. The microhardness evaluation was performed on the metallographic specimen at the middle of the thickness in the transverse direction using a Vickers microhardness tester, model: MVK H1 with an applied load of 500 gf and dwell time of 10 s.

The transverse tensile properties of the FS-welded joints were determined using a computer interfaced universal testing machine, make: Biss (Model No: Bi-04-2360 L1S1, 100 kN capacity), tested at a chuck speed of 5 mm/min in the room temperature conditions. Also, Charpy test specimens with 45° V-notch were prepared as per ASTM A370 standard and tested at room temperature conditions to evaluate the toughness of the weld joint in an impact testing machine. Further, the morphology of fracture surface of typical Charpy test specimens was studied using scanning electron microscope (SEM).

Table 2 Mechanical properties of AISI 316L stainless steel

Density, g/cm^3	Young's modulus, GPa	Ultimate tensile strength (UTS), MPa	Yield strength (YS), MPa	Percentage elongation (PE), %	Hardness, HRB
8	193	630	320	55	79

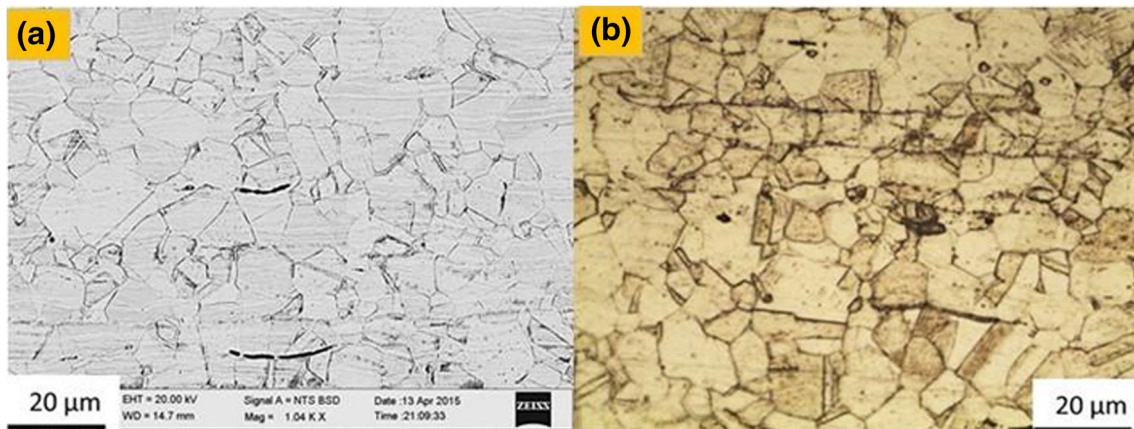


Fig. 1 Typical micrographs of the base steel; a SEM. b OM

3 Results and discussion

3.1 Effect of welding speed on microstructural properties of the weld zone

Figure 3 depicts the surface appearance of the weld joints at different welding speeds. The weld joints produced at 25, 50 and 75 mm/min did not show any external or internal macro defects. However, by examining the weld joint made at welding speed of 100 mm/min using x-ray non-destructive test, a cavity penetrating through the advancing side was evidenced in the welding direction, is a typical tunnel defect that was formed probably due to the insufficient heat input during

FSW [23], as seen in Fig. 4. Owing to the low-heat generation and the resulted low plasticization, the material displaced from the advancing side (AS) to retreating side (RS) was not effectively transferred back to the AS and this possibly led to the formation of tunnel defect at the AS.

Figure 3 also, illustrates the weld bead appearance with ‘C’ streaks. The C streaks are formed for each revolution of the tool with an advancement by certain distance in the welding direction. The streaks are similar and the distance between the two adjoining streaks, so-called weld pitch, will be constant for a typical weld joint. The pitch of the C streaks depends on the welding speed whereas, the legibility of the C streaks was influenced by the plasticization temperature (heat generation), axial force and tool tilt. However, for a given tool rotational speed (N), axial force (F) and tool tilt angle (T), welding speed was responsible for the plasticization temperature and legibility of the C streaks. At lower welding speed, C streaks are less legible and at higher welding speed, the more legible C streaks are formed. But, if the welding speed was increased beyond some limit, the legibility of C streaks decreased due to lack of plasticization temperature and consolidation time. As a result, the weld joint may attribute to produce a defective weld. Ke et al. [24] reported that defect-free weld joints can be obtained when the distance between two consecutive C streaks, so-called weld pitch, are closer, such that weld zone experience optimal level of heat generation for the material transfer. A wider pitch would pave the way to the cavity or tunnel formation, owing to lower heat generation and consequently influence the characteristics of the weld joint. Therefore, the welding speed was found to be a crucial factor responsible for producing defect-free weld joints.

Figure 5 depicts the optical micrographs of the weld SZ of typical FS-welded joints at different welding speeds. For all the welds, the grain size of the weld SZ was lower than the base steel and found to be 14 ± 2 , 7 ± 2 and 3 ± 2 μm at welding speeds of 25, 50 and 75 mm/min, respectively. It was observed that the grain size of the weld SZ decreases with increase in the welding speed and in all the cases the grains

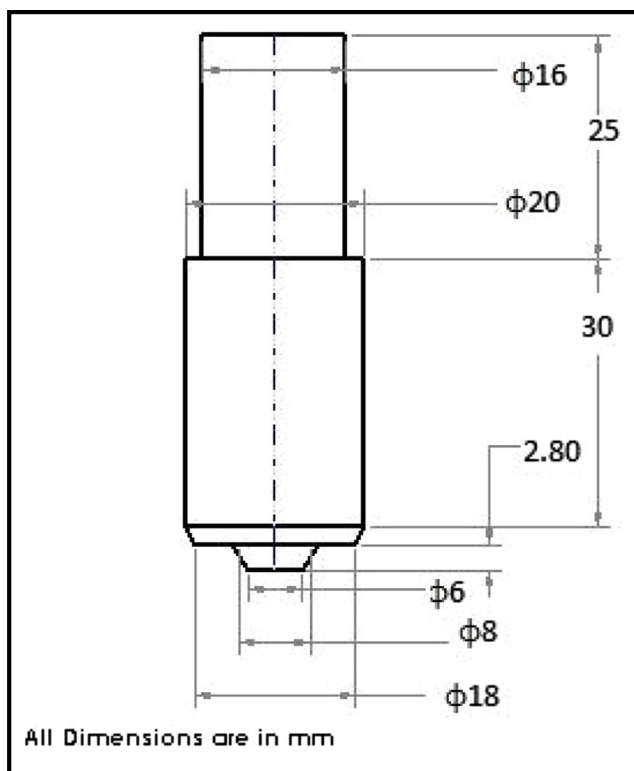
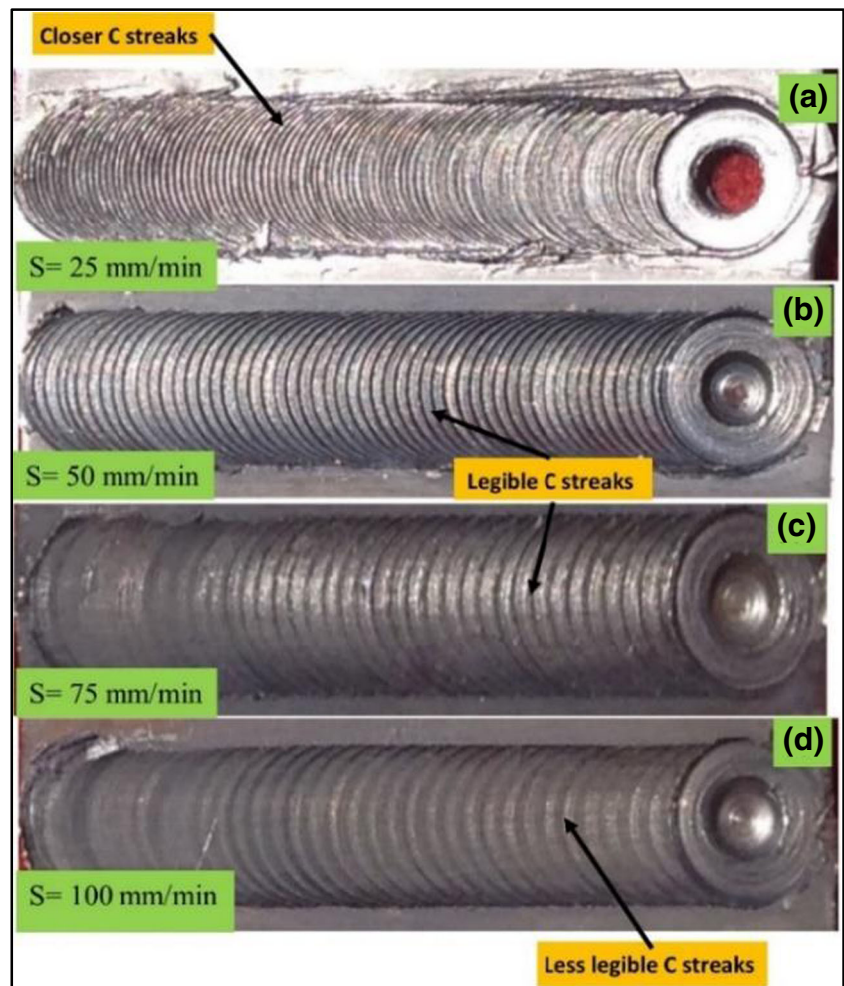


Fig. 2 Geometry of the developed FSW tool

Fig. 3 Surface appearance of a typical set of FS welded joints. **a** 25 mm/min. **b** 50 mm/min. **c** 75 mm/min. **d** 100 mm/min



were roughly equiaxed. The equiaxed grains in the SZ was a clear indication of discontinuous dynamic recrystallization mechanism (DDRX) involved during FSW of austenitic stainless steel and attributed to the nucleation of new strain-free grains [25]. The low-heat generation per unit length with increase in applied strain at higher welding speeds was the reason for the decrease in grain size.

The microstructural properties at the weld SZ is mostly influenced by the peak temperature during FSW. The highest temperature recorded in welds produced at 25, 50, 75 and 100 mm/min were 1164, 975, 798 and 701 °C, respectively. Typical temperature plots as a function of time for weld joints produced at different welding speeds are illustrated in Fig. 6. The temperature recorded would be nearly equal to the actual

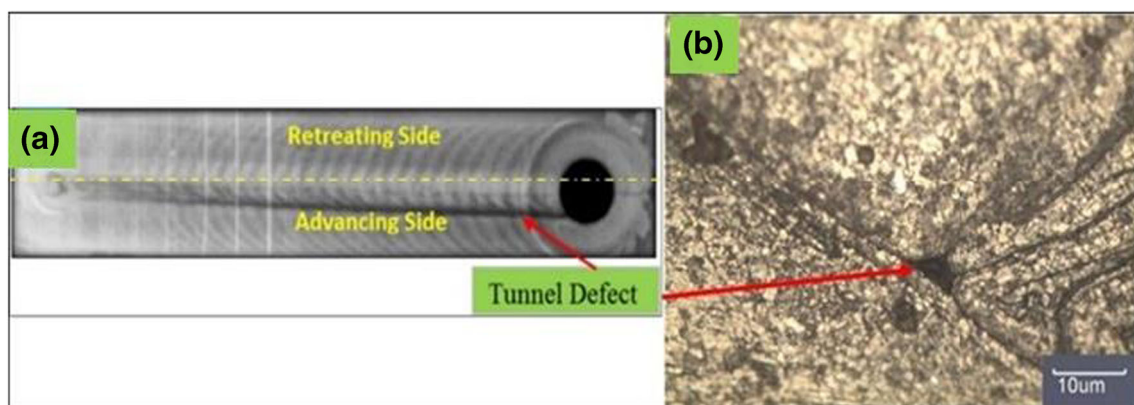


Fig. 4 **a** X-ray radiography image of the joint produced at 100 mm/min. **b** Optical micrograph at the advancing side of the joint produced 100 mm/min

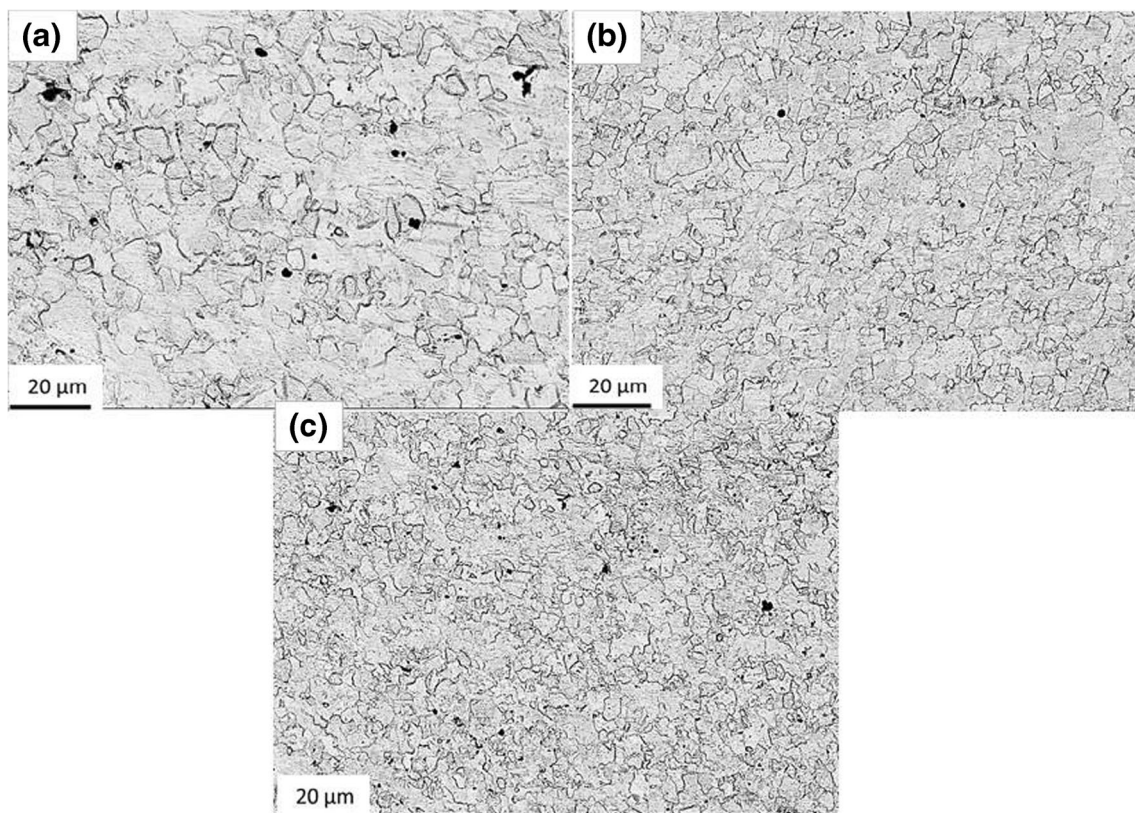


Fig. 5 Optical micrographs of the weld stir zone at **a** 25 mm/min, **b** 50 mm/min and **c** 75 mm/min

temperature at the joint interface (at the middle of the joint) as the thickness of the base steel was only 3 mm.

Apart from peak temperature, the two different mechanisms, namely the rate of heat generation and the rate of material deformation, also govern the microstructure evolution. Increase in heat generation results to coarsening of grain size, whereas increase in deformation rate results reduction in size of the grains. At welding speed of 25 mm/min, the peak temperature was about 80% of the melting temperature of the base steel, where the heat generation was dominant over the

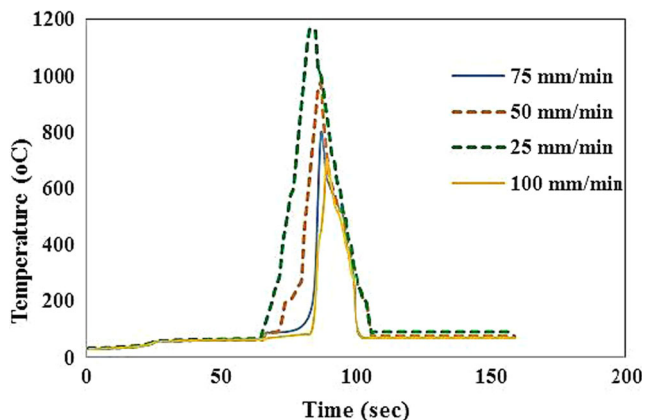


Fig. 6 Typical FSW thermal history plot at welding speeds of 25, 50, 75 and 100 mm/min

deformation rate. The nucleated grains underwent grain coarsening owing to slow transverse speed of the tool experiencing higher heat generation per unit length of the weld. As a result, the grains absorbed more heat under the influence of the tool shoulder and coarser grains were evolved in the weld SZ. At welding speed of 50 mm/min, the maximum welding temperature recorded was about 67% of the melting temperature of the base steel. The decrease in heat generation and the increase in rate of material deformation led to the reduction in grain size at the weld SZ. Interestingly, the average grain size was approximately half of the average grain size in the SZ of the joint produced at welding speed of 25 mm/min. However, at 75 mm/min, the SZ depicted a fine refinement of the grains in the weld SZ. The lower welding temperature (about 55% of the melting temperature of the base steel) and the higher material deformation rate at 75 mm/min could be the probable cause for the above microstructural feature. Also, the cumulative effect of lower heat generation and increase in material deformation rate on grain refinement is more significant at higher welding speeds.

Figure 7 depicts the EBSD-IPF image of the SZ of the weld joint produced at welding speeds of 25, 50 and 75 mm/min. The presence of equiaxed grains interspersed with deformed grains confirms the occurrence of DDRX in the SZ. The material flow ascribes a typical simple shear deformation of the grains in the weld SZ and probably as a result most of the

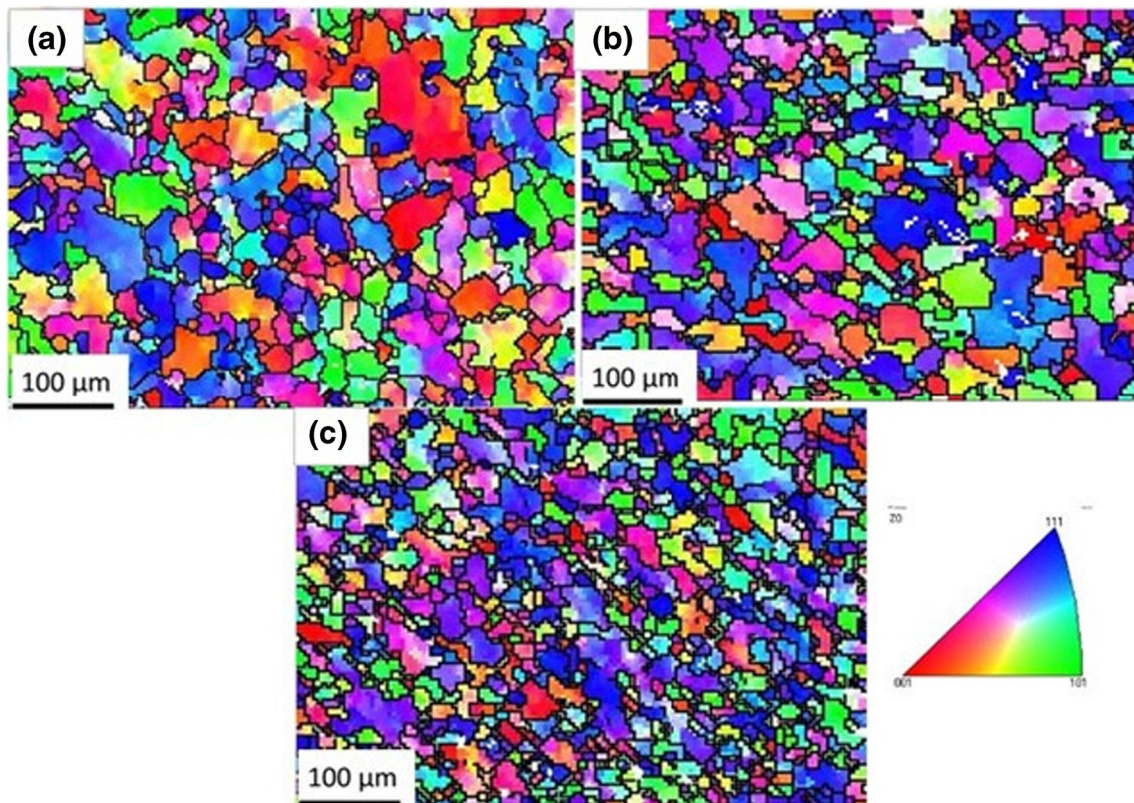


Fig. 7 Typical EBSD-IPF image of the stir zone for joints produced at welding speed of **a** 25 mm/min, **b** 50 mm/min and **c** 75 mm/min

refined grains are presumably rotated to 111 shear plane orientation, a typical characteristic of the FCC material (base steel). Grain boundary misorientation diagrams were used to study the deformation of the grains at the weld SZ with regard to change in the welding speed as depicted in Fig. 8. At 25 mm/min, the boundary fraction of the low- and high-angle grain boundaries at the SZ was 58 and 42%, respectively. But, at 50 and 75 mm/min, the boundary fraction of low-angle grain boundaries was increased to 77 and 90% with decrease in the fraction of high-angle boundaries to 23 and 10%, respectively. The higher fraction of low-angle grain boundaries at higher welding speeds signifies that DDRX was the dominant recrystallization mechanism at the SZ during the FSW process.

Away from the SZ, distinct TMAZ were observed on either side, where the grains are partially dislocated by the influence of thermo-mechanical effects of the tool pin and shoulder. Figure 9 depicts typical optical micrographs of the TMAZ on the advancing side of the joints. The average grain size in the TMAZ of welds produced at welding speeds of 25, 50 and 75 mm/min was found to be 16 ± 2 , 10 ± 2 and 7 ± 2 μm , respectively. The formation of sub-grain boundaries was more predominant in the TMAZ region. However, relatively low temperature in this zone influences wider grain dislocations and adversely affect the recovery of the dislocated grains. Austenitic stainless steels are classified among medium to

low stacking fault energy (SFE) material and therefore, the low SFE of the base steel, also, affects the recovery of the dislocated grains. As a consequence, the dislocations can hardly rearrange themselves into sub boundaries and thus pile up inside the grains [26].

Unlike carbon steel, stainless steel does not have transformation (i.e. from 1100 °C to room temperature) and thus, the features of recrystallization are believed to remain intact after FSW. Thus, even at low-temperature recrystallization process (0.55 times the melting temperature of the base steel at 75 mm/min), mostly austenite grain boundaries were distributed in the weld SZ. But, during FSW at 25 mm/min, the relatively higher welding temperature (0.8 times the melting temperature of the base steel) and cooling rate in the weld SZ are believed to greatly influence the phase change and material properties of the base steel. Figure 10 illustrates the Fe–Cr–Ni pseudo-binary diagram of the base AISI 316L stainless steel. The chromium and nickel equivalents were determined from the Schaeffler relationships [27], using Eqs. (1) and (2).

$$\text{Cr}_{\text{eq}} = \text{Cr} + \text{Mo} + 1.5 \text{Si} + 0.5 \text{Nb} \quad (1)$$

$$\text{Ni}_{\text{eq}} = \text{Ni} + 0.5 \text{Mn} + 30 (\text{C} + \text{N}) \quad (2)$$

From the phase diagram, it is found that the peak temperature during FSW at welding speed of 25 mm/min lies near the

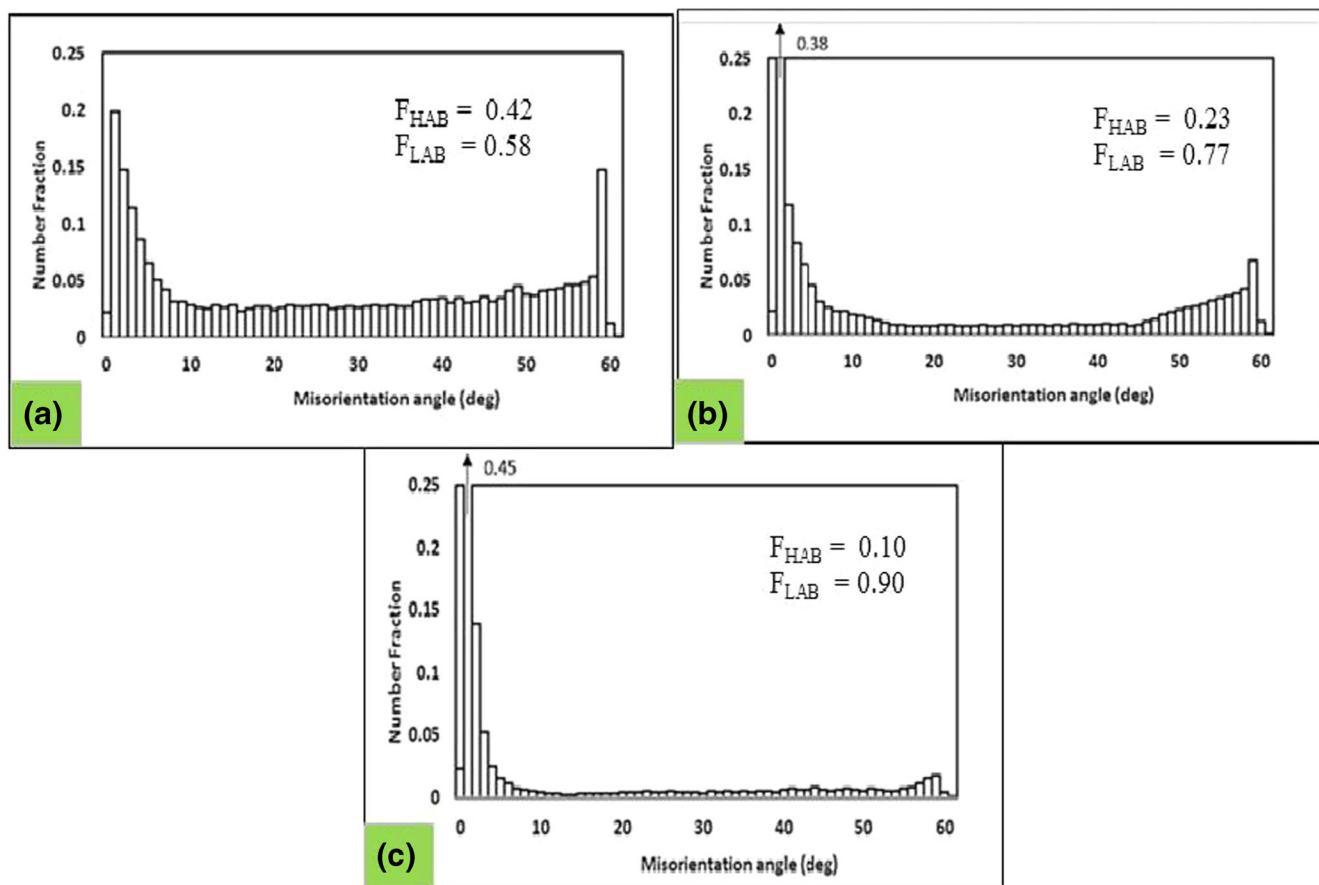


Fig. 8 Grain boundary misorientation details at the weld SZ of the joint made at **a** 25 mm/min, **b** 50 mm/min and **c** 75 mm/min

region of ($\delta + \gamma$) indicating the possibility of the delta ferrite existence in the weld SZ. Thus, the microstructural features of the SZ at welding speed of 25 mm/min were explored using SEM, TEM and XRD. The TEM and SEM-EDS analysis shown in Fig. 11a, b confirm the emergence of delta ferrite with thin flake-like structure between austenite grain boundaries [28]. The delta ferrite would emerge when the SZ temperature exceeded the transformation temperature ($\delta + \gamma$) region such that the ferrite stabilizing elements like chromium and molybdenum transform more into ferrite phase by decreasing the austenite stabilizing elements like nickel and nitrogen (i.e. paramagnetic material property of the austenite was transformed to ferromagnetic property of the delta ferrite). The result of EDS analysis of the area (Fig. 11b) confirmed the presence of the following elements; Fe = 69.50%, Cr = 21.85%, Ni = 6.63%, Mo = 2.04% and N = 0.03% (wt%). The higher concentration of chromium and the lower concentration of nickel in comparison to the base steel is a clear indication of delta ferrite formation in the weld SZ.

In order to estimate the amount of delta ferrite in the weld SZ, a ferritescope (model: mp30) was used. The amount of delta ferrite in the weld SZ was found to be $7.21 \pm 0.45\%$. The results of the EDS analysis at welding speed of 25 mm/min was validated by XRD analysis and a typical XRD spectrum is

shown in Fig. 12. The intensity (counts)-the peaks of higher and lower intensity confirmed the presence of austenite and delta ferrite phases in the weld SZ. However, no sign of sigma phase was detected in the XRD analysis. No delta ferrite was observed in the SZ of the weld joint produced at welding speeds of 50 and 75 mm/min, probably due to the lower peak temperature and faster cooling rate of the weld zone.

Beside δ -ferrite, sigma phase evolution is believed to have a great influence on the weld joint characteristics of austenitic stainless steels. The sigma phase has a body cubic tetragonal structure, and its precipitation temperature is perceived between 600 and 1000 °C [29]. The lattice constants a_o and c_o of sigma phase in AISI 316L stainless steel are 0.921 and 0.478 nm, respectively [10]. The sigma phase mostly precipitate in the ferrite grain boundaries, as the preferential sites for the nucleation in case of austenitic stainless steels. The precipitation potential of sigma phase in high Cr-rich regions (i.e. delta ferrite) was estimated about 100 times than that in the austenite phase regions. Only a few researchers have reported the precipitation of sigma phase during FSP [20] and FSW [30, 31] of austenitic stainless steels. The authors speculate that the sigma phase precipitation was due to the emergence of δ -ferrite at higher welding temperatures experiencing severe strain in the material during frictional stirring, which

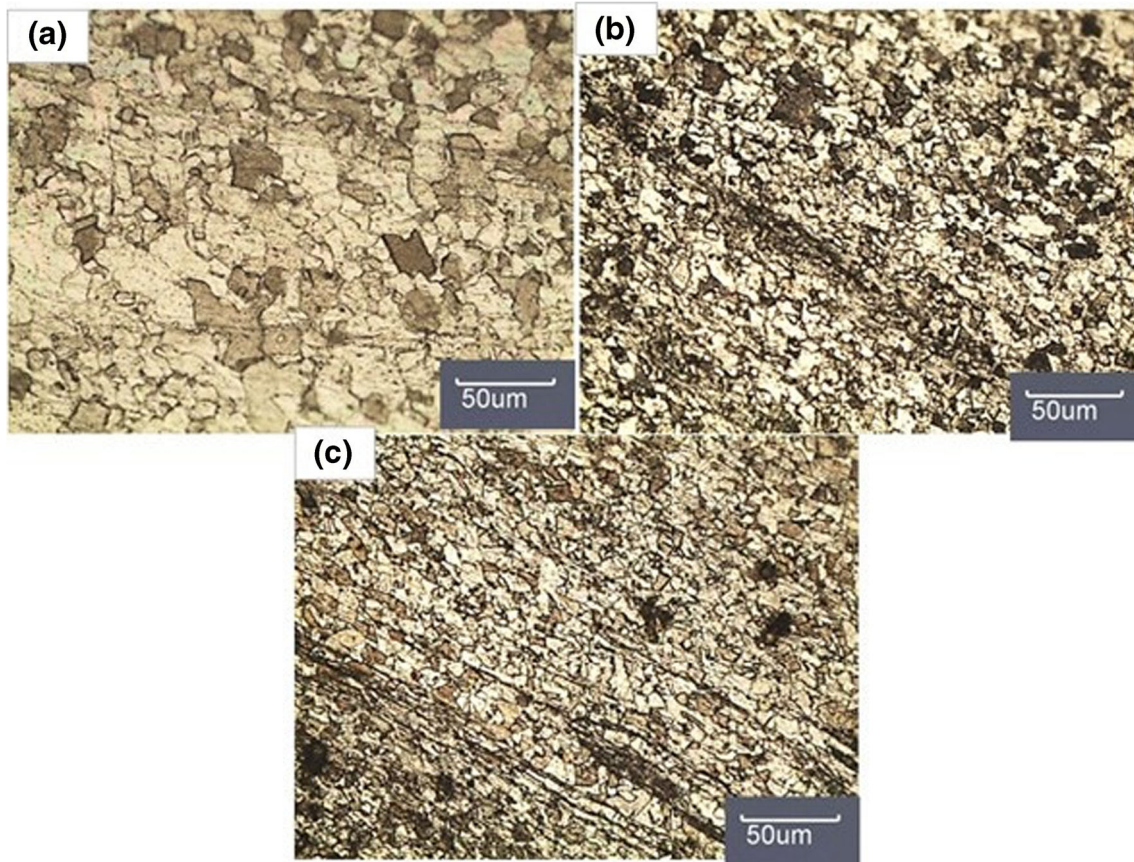


Fig. 9 Optical micrographs of the TMAZ on the advancing side. a 25 mm/min. b 50 mm/min. c 75 mm/min

subsequently led to the decomposition of delta ferrite to sigma phase during the cooling thermal cycle [32]. Therefore, the weld SZ of the joint produced at 25 mm/min was examined using XRD and TEM for the possible existence of sigma

phase. But, in both methods, sigma phase precipitation was not observed in the weld SZ. This may be due to the fact that delta ferrite has probably not decomposed to sigma phase owing to the relatively faster cooling of the weld SZ (due to low thickness of the base steel plate). Kokawa and co-researchers [18], also, reported that delta ferrite was retained in the SZ because of the higher cooling rate during friction stir processing (FSP) of 2-mm-thick 304 stainless steel. But, in the case of FSP of 6-mm-thick 304 stainless steel, the authors found that the delta ferrite was decomposed to sigma phase owing to relatively slower cooling rate. The studies carried out by Villanueva et al. [33] claims that the precipitation of sigma phase in AISI 316L was especially observed at the δ/γ (i.e., delta ferrite/ austenite) interface boundaries as the preferential sites for nucleation during ageing. As the ageing temperature was increased, the sigma phase precipitates were observed at the triple point as well as at the δ/γ interface boundaries. It was also reported that the decomposition of the delta ferrite to sigma phase during ageing at 700 °C had taken a minimum of 0.5 h, which is too longer a period to happen in any FSW process. Further, the joint interface region was also examined using micro etchants such as Groesbeck and modified Murakami reagents for the possible existence of sigma phase [22] and confirmed that no sigma phase precipitation in the weld SZ.

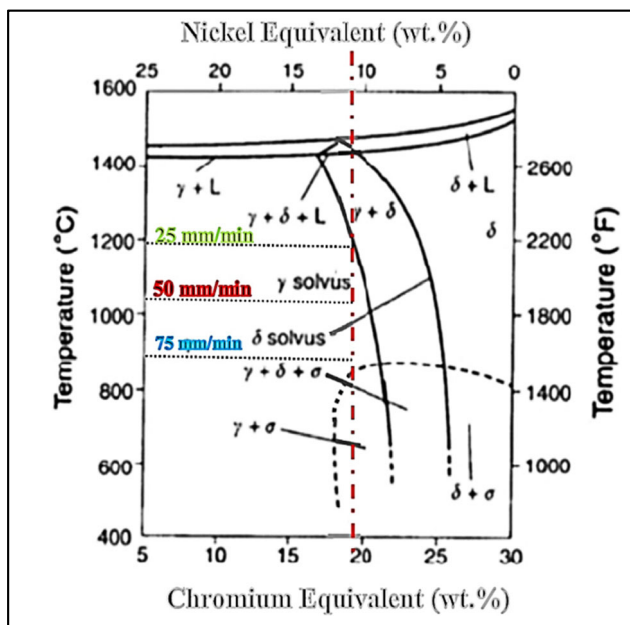
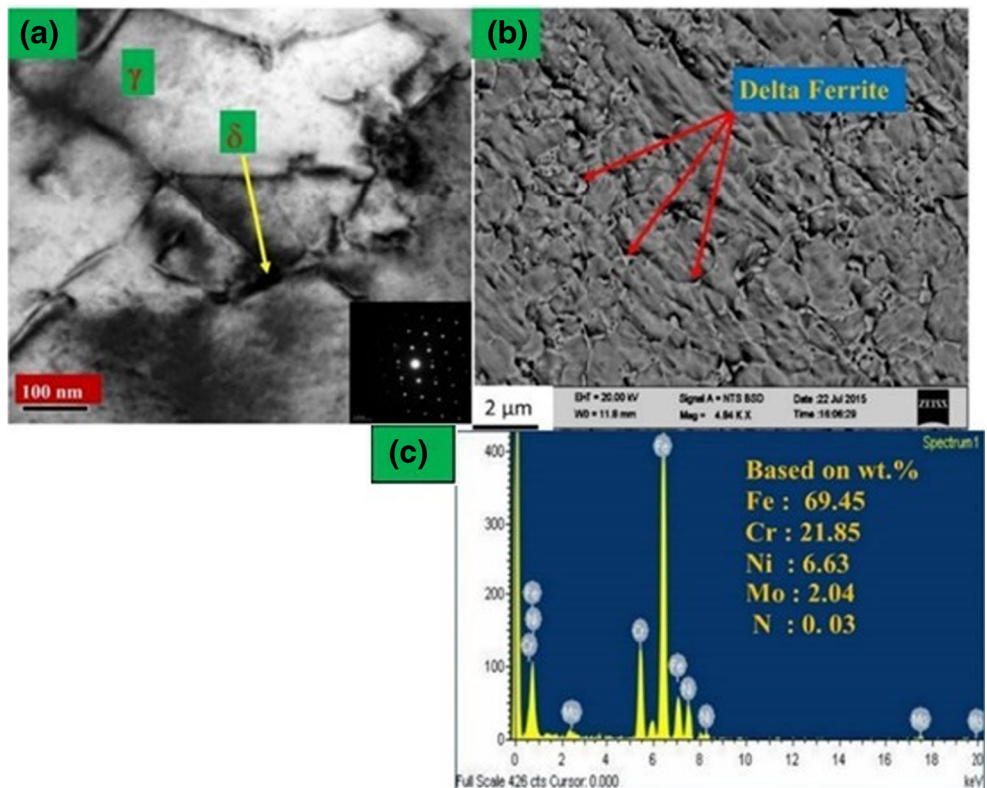


Fig. 10 Fe–Cr–Ni ternary system for 70% Fe [27]

Fig. 11 Microstructure of weld stir zone of the joint produced at 25 mm/min. **a** TEM image of δ -ferrite and austenite (γ). **b** SEM image of δ -ferrite island in the matrix of austenite. **c** Corresponding EDS analysis



3.2 Effect of welding speed on impact strength of the joints

Table 3 presents the values of toughness of the weld joints produced at different welding speeds as obtained by Charpy test (tested at room temperature condition). The test results reveal that all the weld joints have lower toughness than the base steel. However, the weld joint made at 75 mm/min exhibited nearly similar toughness as that of the base steel.

For all the welds, the fracture occurred from the centre of the V-notch towards the retreating side of weld. The SEM-BSE images of typical fractured Charpy specimens are shown in Fig. 13. The fracture surface morphology clearly indicates (mostly) ductile mode of failure in all the cases. At welding speed of 25 mm/min, the fracture morphology shows elongated quasi-cleavage surface with the presence of voids. Elongated quasi-cleavage surface was the result of high localized heating and voids are formed probably due to improper

Fig. 12 XRD spectrum of the weld zone of the joint produced at 25 mm/min

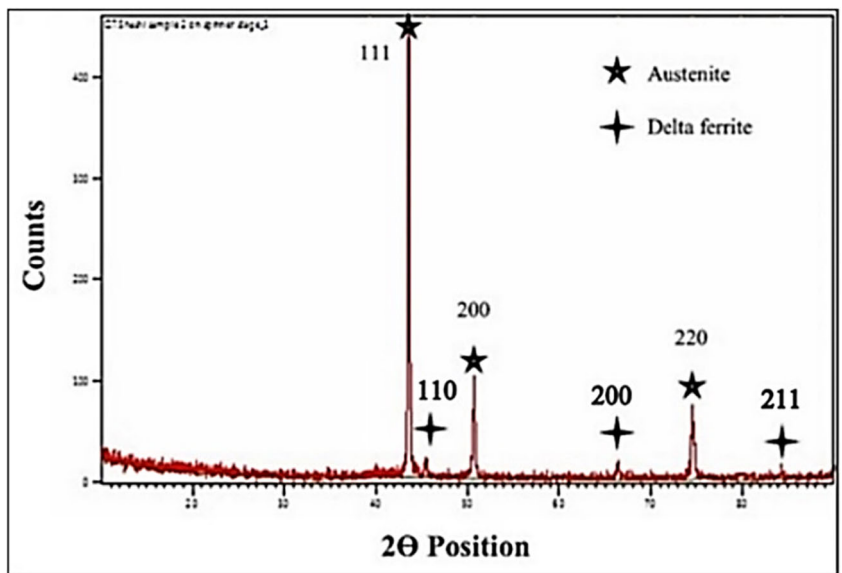


Table 3 Evaluated toughness of Charpy specimens of the joints at different welding speeds

Welding speed (mm/min)	25	50	75	Base metal
Toughness (J/cm ²)	39 ± 0.30	48 ± 0.43	49 ± 0.54	50 ± 0.15

material coalescence. The formation of delta ferrite was the probable cause for the lower toughness of the weld joints. At 50 mm/min, the fracture morphology was highly fibrous with more population of dimple throughout, probably due to the near optimal level of heat generation and material strain rate. Therefore, the higher joint toughness observed at 50 mm/min was quite rational. At 75 mm/min, the high population of fine fibrous dimple structure was wide spread probably as a consequence of the lower heat generation. However, possibly due to the increase in rate of deformation, the cleavage surface was observed rarely between the highly fibrous dimple surfaces. Therefore, the predominant fibrous dimples with rarely observed cleavage surface on the fracture surface substantiate the slight reduction in toughness of the joint produced at 75 mm/min to that of the base steel toughness.

3.3 Effect of welding speed on microhardness of the joints

The microhardness distribution across the weld zone at welding speeds of 25, 50 and 75 mm/min is shown in Fig. 14. The base metal exhibits some uncertainty in hardness, as they are originally subjected to cold rolling and solution annealing treatments and its value was equal to 190 ± 5 HV. For all the welds, the microhardness of the weld SZ was significantly higher than the base steel hardness. The highest microhardness of 275 HV was observed in the SZ of the weld produced at welding speed of 75 mm/min. At 75 mm/min, the evolution of fine equiaxed grains in the weld SZ could be the probable reason for higher hardness. Away from the SZ, in the TMAZ on either side also, higher hardness was observed. In the TMAZ, formation of deformed grains and sub-grain boundaries are inherent characteristics. However, the rearrangement of sub-grains between deformed grains could be the probable cause for the relatively better hardness at the TMAZ than the base steel. At welding speeds of 25 and 50 mm/min, a low hardness region was observed near the transition region of TMAZ and HAZ at the RS of the joints. This may be probably due to lack of material coalescence in the transition zone of the joint. But, at 75 mm/

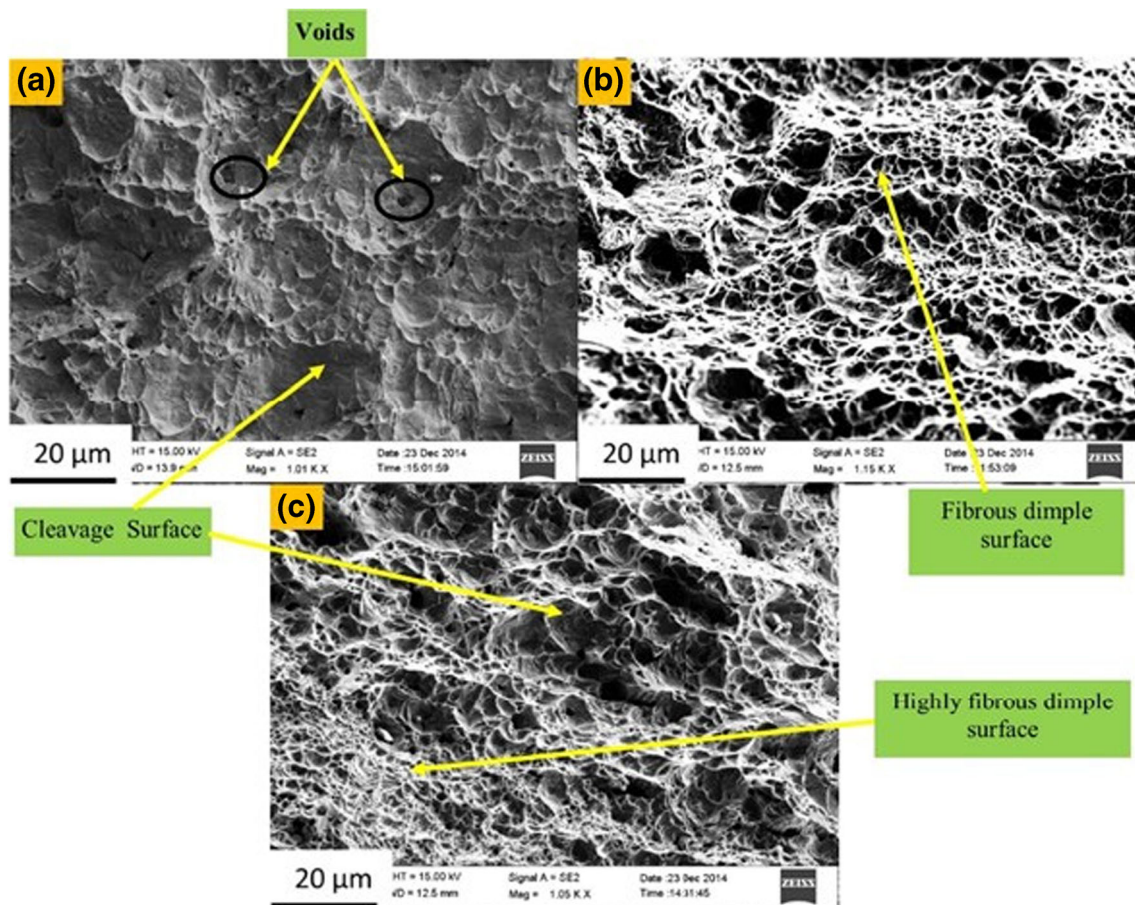
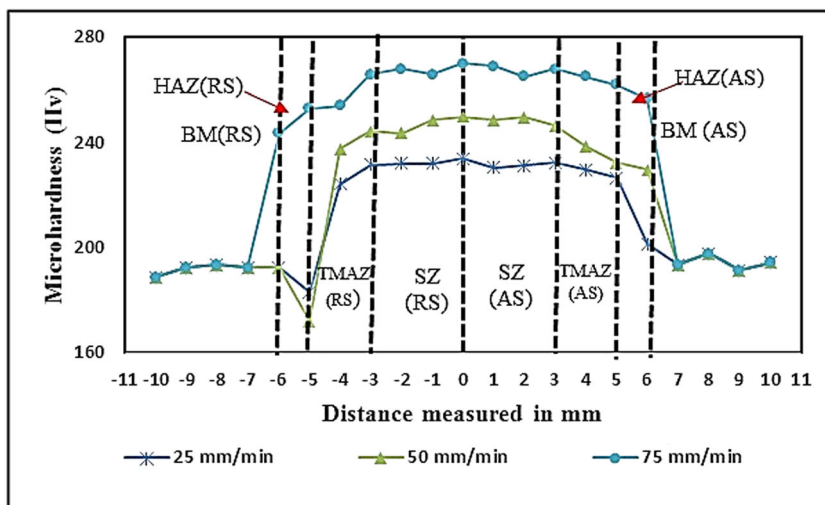


Fig. 13 SEM fractographs of the Charpy specimens at welding speeds of **a** 25 mm/min, **b** 50 mm/min and **c** 75 mm/min

Fig. 14 Microhardness distribution across the FS-welded joints



min, no such low hardness regions were observed. As discussed above, the relatively higher microhardness observed in the weld SZ was primarily due to decrease in grain size. The microhardness distribution at the SZ is consistent with the Hall-Petch relationship, where the grain size decreased for increase in welding speeds. Figure 15 depicts the correlation between the Vickers microhardness and grain size of SZ at different welding speeds. The linear relationship portrayed in the plot is given in Eq. (3)

$$HV = 219.27 d^{-1/2} + 169.18 \tag{3}$$

where HV = Vickers microhardness and d = grain size at the SZ.

3.4 Effect of welding speed on tensile properties of the joints

The evaluated transverse tensile properties of the FS-welded 316L stainless steel joints are shown in Fig. 16. All the weld

joints exhibited higher yield strength (YS) compared to that of the base metal. The observed joint yield strength was 467, 555 and 579 MPa at welding speed of 25, 50 and 75 mm/min, respectively, and the base steel has a yield strength of 320 MPa. The significantly higher joint yield strength was mainly due to the refinement of grains in the SZ of the joints. During the dynamic recrystallization process in the SZ, the mean travel distance of the dislocation decreases and soon starts pile up of dislocations at grain boundaries [34]. This also contribute for the increase in yield strength of the FS-welded joints.

The ultimate tensile strength (UTS) of the weld joints are 542, 610 and 632 MPa at welding speeds of 25, 50 and 75 mm/min. At 25 and 50 mm/min, the weld joint strength was only 86 and 97% of the base steel UTS. But, the UTS of the joint made at 75 mm/min depicted a higher strength than the base steel. In all cases, the location of fracture was away from the weld SZ. A typical set fractured tensile specimen is shown in Fig. 17. At 25 mm/min, the fracture location was in the HAZ at the RS of the joint. The fracture location was consistent with the microhardness distribution as discussed above. As observed in Fig. 3a, the wider bead at 25 mm/min thinned down

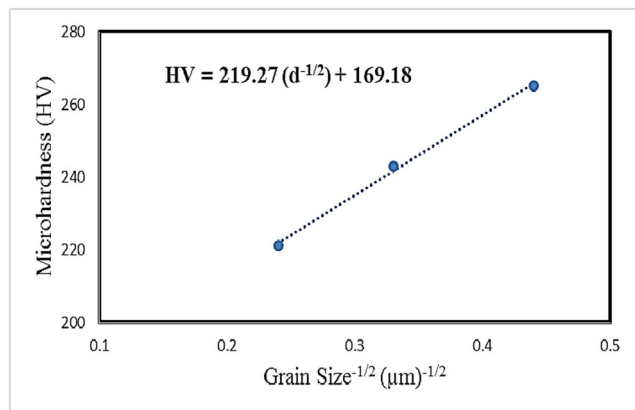


Fig. 15 Hall-Petch relationship between microhardness and the grain size in the SZ

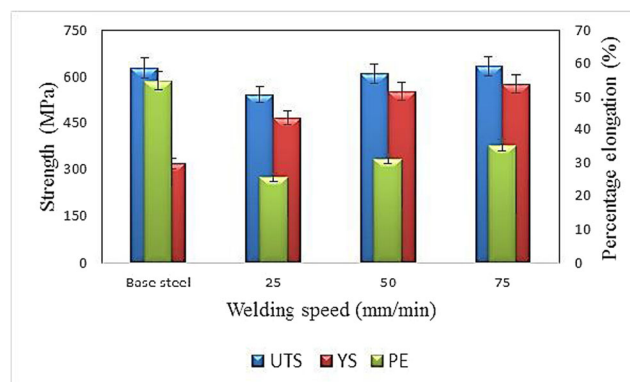
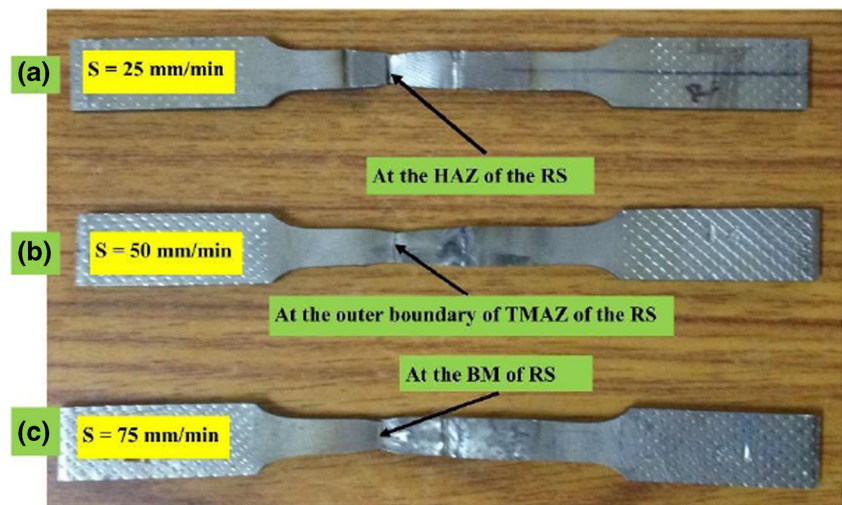


Fig. 16 Evaluated tensile properties of FS-welded 316L stainless steel joints

Fig. 17 Typical set of fractured tensile specimens **a** at 25 mm/min, **b** at 50 mm/min and **c** at 75 mm/min



the thickness of SZ owing to the shoulder plunge and as a result, the RS became the weakest part. This fact, together with the coarse grains, might have caused the fracture of the transverse tensile test specimen in the HAZ at the RS. At 50 mm/min, the location of fracture was at the outer boundary of the TMAZ of the RS of the weld joint. The low dislocation density of grains at the outer boundary of the TMAZ of the RS could be the probable reason for marginal reduction in the weld joint strength. But, at 75 mm/min, the location of fracture was at the base steel. The decrease in the grain boundary migration, owing to high dislocation density of grains, could be the reason for the strengthening of the weld zone.

It was clear that the mechanical properties of the weld joints are influenced by the grain size and the resultant microstructural phase during FSW. At lower welding speed, the presence of delta ferrite in the weld stir zone decreased the hardness as well as the strength of the joint; but with increase in the transverse speed, the evolution of equiaxed austenite grain boundaries increased the joint strength as well as the hardness of the FS-welded joints. However, the ductility of the joints in all the cases was lower than that of the base steel. The limited ductility in the weld SZ was associated with reduction in the grain size and the strain hardening characteristics of the base steel. The increase in the strain-hardening exponent decrease the mean free path of the dislocation motion and further accelerate dislocations accumulation against grain boundaries [35].

4 Conclusions

From the mechanical and metallographic characterization of the joints, the following key conclusions are derived.

- The welding speed has significant influence on the microstructure evolution in the weld zone and hence on the joint strength and toughness.

- With increase in welding speed, the average grain size of the weld stir zone (SZ) decreased drastically and at 75 mm/min, the average SZ grain size is $3 \pm 2 \mu\text{m}$ against the base metal grain size of $28 \pm 5 \mu\text{m}$.
- The grain refinement in the SZ was preceded by discontinuous dynamic recrystallization (DDRX) mechanism and the evolution of fine and equiaxed grains in the SZ at 75 mm/min resulted in joint strength more than that of the base steel. The tensile strength and toughness at 75 mm/min are 632 MPa and 49 J/cm², respectively. The tensile strength and toughness of the base steel are 630 MPa and 50 J/cm², respectively.
- Considering strength and toughness of the joints and productivity, higher welding speeds are conducive. But, when the welding speed exceeds certain limit, lack of material plasticization and coalescence lead to internal tunnel defects.
- The microhardness at the SZ increases with increase in welding speed and this observation was in good agreement with the well-known Hall-Petch relationship between welding speed and microhardness.
- At low welding speeds, the formation of delta ferrite was confirmed in the weld SZ, but no sign of precipitation of sigma phase was observed anywhere in the weld zone at any welding speeds.

Funding information The authors wish to place on record their sincere thanks to the Directorate of Extramural Research and Intellectual Property Rights, DRDO, Govt. of India, for providing funds for carrying out the investigation (vide funded project: Ref. No. ERIP/ER/1102200/M/01/1465 Dated 29.01.2013).

References

1. Ishino S (1996) History, progress, achievements and future prospect of research activities on fusion materials by Japanese university researchers. *J Nucl Mater* 233-237:1535–1540

2. Lakshminarayan AK (2016) Enhancing the properties of friction stir welded stainless steel joints via multi-criteria optimization. *Arch Civ Mech Eng* 16:605–617
3. Yan J, Goa M, Zeng X (2010) Study on microstructure and mechanical properties of 304 stainless steel joints by TIG, laser and laser-TIG hybrid welding. *Opt Laser Eng* 48(4):512–517
4. Feng Y, Luo Z, Liu Z, Li Y, Luo Y, Huang Y (2005) Keyhole gas tungsten arc welding of AISI 316L stainless steel. *J Mater Des* 85: 24–31
5. Kocabekir B, Kacar R, Gunduz S, Hayat F (2008) An effect of heat input, weld atmosphere and weld cooling conditions on the resistance spot weldability of 316L austenitic stainless steel. *J Mater Process Technol* 195:327–335
6. Gowrishankar I, Bhaduri AK, Seetharaman V, Verma DDN, Achar DRG (1987) Effect of number of passes on the structure and properties of submerged arc welds of AISI type 316L stainless steel. *Weld J* 66:147s–154s
7. Shankar V, Gill TPS, Mannan SL, Sundaresan S (2003) Solidification cracking in austenitic stainless steel welds. *Sadhana* 28(3–4):359–382
8. Kadoi K, Fujinaga A, Yamamoto M, Shinozaki K (2013) The effect of welding conditions on solidification cracking susceptibility of type 310 S stainless steel during laser welding using an in-situ observation technique. *Weld World* 57(3):383–390
9. Karlsson L, Arcini H (2012) Low energy input welding of duplex stainless steels. *Weld World* 56:41–47
10. Lo KH, Shek CH, Lai JKL (2009) Recent developments in stainless steels. *Mater Sci Eng R* 65:39–104
11. Beltran R, Maldonado JG, Murr LE (1997) Effects of strain and grain size on carbide precipitation and corrosion sensitization behaviour in 304 stainless steel. *Acta Mater* 45(10):4351–4360
12. Almanza E, Murr LE (2000) A comparison of sensitization kinetics in 304 and 316 stainless steels. *J Mater Sci* 35:3181–3188
13. Cross HJ, Faux SP, Sadhra S, Sorahan T, Levy LS, Aw TC, Braithwaite R, McRoy C, Hamilton L, Calvert I (1997) Criteria document for hexavalent chromium. International Chrome Development Association (ICDA), Paris
14. Commission VIII “Health, safety and environment” of the IHW (2011) Lung cancer and arc welding of steels. *Weld World* 55(11–12):12–20
15. Thomas WM, Nicholas ED, Needham JC, Murch P, Temple-Smith P, Dawes CJ (1991) Friction stir butt welding. GB Patent Application No. 9125978.8, International Patent Application PCT/GB92/02203, 6 December 1991
16. Meshram MP, Kumar Kodli B, Dey SR (2014) Friction stir welding of austenitic stainless steel by PCBN tool and its joint analyses. *Procedia Mater Sci* 6:135–139
17. Meran C, Kovan V, Alptekin A (2007) Friction stir welding of AISI 304 austenitic stainless steel. *Mater Sci Technol* 38(10):829–835
18. Kokawa H, Park SHC, Sato YS, Okamoto K, Hirano S, Inagaki M (2005) Microstructures in friction stir welded 304 austenitic stainless steel. *Weld World* 49(3/4):34–40
19. Meran C, Canyurt OE (2010) Friction stir welding of austenitic stainless steels. *J Achiev Mater Manuf Eng* 43(1):432–439
20. Chen YC, Fujii H, Tsumura T, Kitagawa Y, Nakata K, Ikeuchi K, Matsubayashi K, Michishita Y, Fujiya Y, Katoh J (2009) Friction stir processing of 316L stainless steel plate. *Sci Technol Weld Join* 14(3):197–201
21. Hajian M, Abdollah-zadeh A, Rezaei-Nejad SS, Assadi H, Hadavi SMM, Chung K (2015) Microstructure and mechanical properties of friction stir processed AISI 316L stainless steel. *J Mater Des* 67: 82–94
22. Shashi Kumar S, Murugan N, Ramachandran KK (2016) Influence of tool material on mechanical and microstructural properties of friction stir welded 316L austenitic stainless steel butt joints. *Int J Ref Met Hard Mater* 58:199–205
23. Kim YG, Fujii H, Tsumura T, Kawasaki T, Nakata K (2006) Three defect types in friction stir welding of aluminium die casting alloy. *Mater Sci Eng A* 415:250–254
24. Liming K, Xing L, Indacochea JE (2004) Material flow pattern and cavity model in friction stir welding of aluminium alloys. *Metall Mater Trans B Process Metall Mater Process Sci* 358:153–157
25. Dieter GE (1988) *Mechanical metallurgy*, second edn. McGraw-hill book company, London, pp 184–197
26. Nandan R, Debroy T, Bhadeshia H (2008) Recent advances in friction-stir welding—process, weldment structure and properties. *Prog Mater Sci* 53(6):980–1023
27. Lippold JC, Kotecki DJ (2005) *Welding metallurgy and weldability of stainless steels*. Wiley-Interscience, John Wiley & Sons, New Jersey
28. Cui HB, Xie GM, Luo ZA, Wang GD (2016) Microstructural evolution and mechanical properties of the stir zone in friction stir processed AISI201 stainless steel. *J Mater Des* 106:463–475
29. Hsieh CC, Wu W (2012) Overview of intermetallic sigma (s) phase precipitation in stainless steels. *Int Scholarly Res Network Metall* 16:1–78
30. Sabooni S, Karimzadeh F, Enayati MH, Ngan AHW, Jabbari H (2015) Gas tungsten arc welding and friction stir welding of ultra-fine grained AISI 304L stainless steel: microstructural and mechanical behavior characterization. *Mater Charact* 109:138–151
31. Park SHC, Sato YS, Kokawa H, Okamoto K, Hirano S, Inagaki M (2005) Corrosion properties in friction stir welded 304 austenitic stainless steel. *Weld World* 49(3–4):63–68
32. Park SHC, Sato YS, Kokawa H, Okamoto K, Hirano S, Inagaki M (2003) Rapid formation of the sigma phase in 304 stainless steel during friction stir welding. *Scr Mater* 49:1175–1180
33. Villanueva DME, Junior FCP, Plaut RL, Padilha AF (2006) Comparative study on sigma phase precipitation of three types of stainless steels: austenitic, ferritic and duplex stainless steel. *J Mater Sci Technol* 22(9):1098–1104
34. Humphreys FJ, Hatherly M (1995) *Recrystallization and related annealing phenomena*, Second edn. Pergamon Press, New York, pp 415–467
35. Kruml T, Polak J, Orbtlik K (1997) Dislocation structures in the bands of localized cyclic plastic strain in austenitic 316L and austenitic ferritic duplex stainless steels. *Acta Mater* 45:5145–5151